Extended data Fig. 1

a

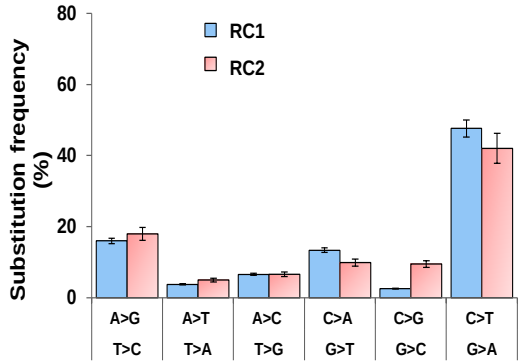

b

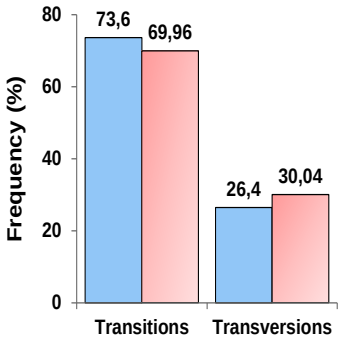

c

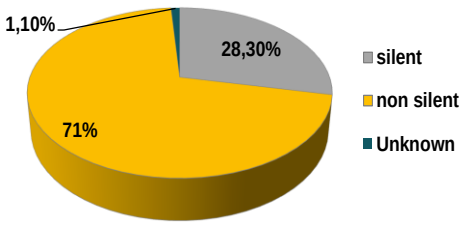

d

GENETIC ALTERATION	RC1	RC2
missense	961	1003
splicing	33	22
stop gain /Fs ins/start cod	47	39
stop loss	4	0
unknown	11	14
Total	1056	1078

Extended data Fig 1. Whole exome sequencing analysis of two rhabdoid colorectal cancers (RC). a Frequency of nucleotide substitutions for the six possible mutation classes. **b** Frequency of substitutions, transitions vs. transversions. **c** Distribution of non-silent somatic mutations in both cancers. **d** Frequency of coding nonsynonymous somatic mutations for each cancer. Error bars are indicated by standard deviation of the mean (s.e.m)

Extended data Fig. 2

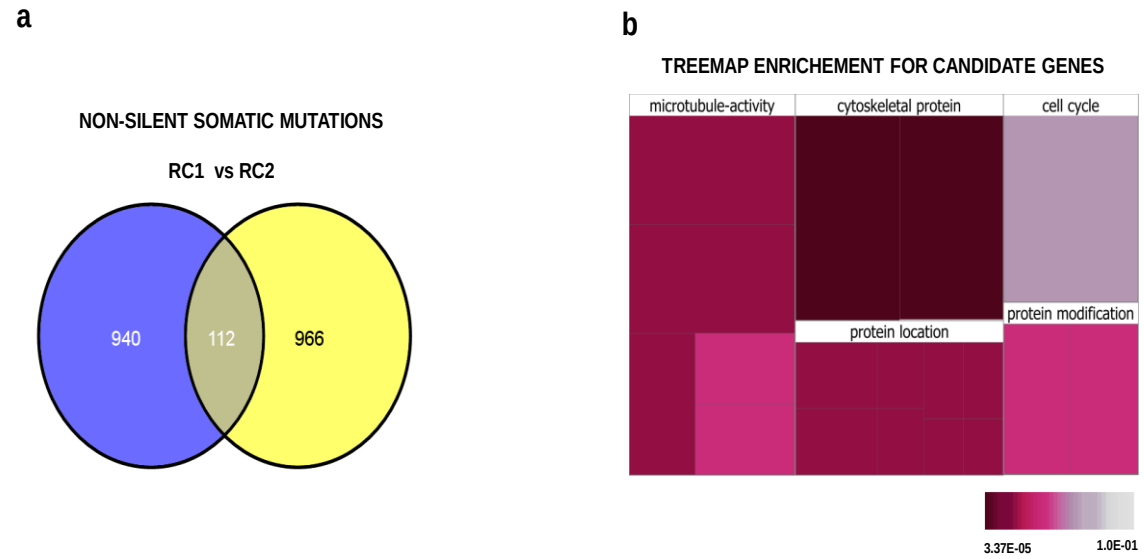

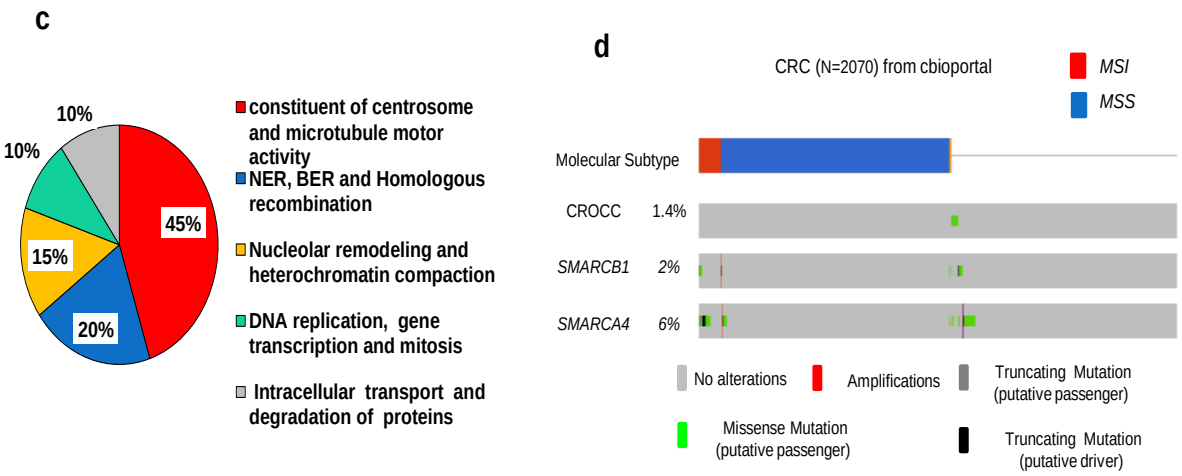

Extended data Fig 2. Non-silent somatic mutations in rhabdoid tumours are enriched in centrosome-microtubule components. a Number and distribution of coding non-silent somatic mutations across the two rhabdoid colorectal cancer samples. **b** enrichment for Gene Ontology (GO) biological processes among the candidate genes shared by the two rhabdoid tumours is shown by using treemap. **c** Colours represent the biological processes in terms of enrichment for the indicated categories. **d** Recurrence of *CROCC*, and known rhabdoid-related genes *SMARCB1 and SMARCA4* across multiple datasets of classical colorectal cancer stratified in Microsatellite instable (MSI) and stable (MSS) subtypes. Samples are derived from 4 studies. Targeted sequencing of 1134 samples from metastatic colorectal cancer samples (MSK, Cancer Cell 2017); Colorectal Adenocarcinoma Triplets (MSKCC, Genome Biol 2014); Colorectal Adenocarcinoma (TCGA); Colorectal Adenocarcinoma (DFCI, Cell Reports 2016).

Supplemental Fig. 3

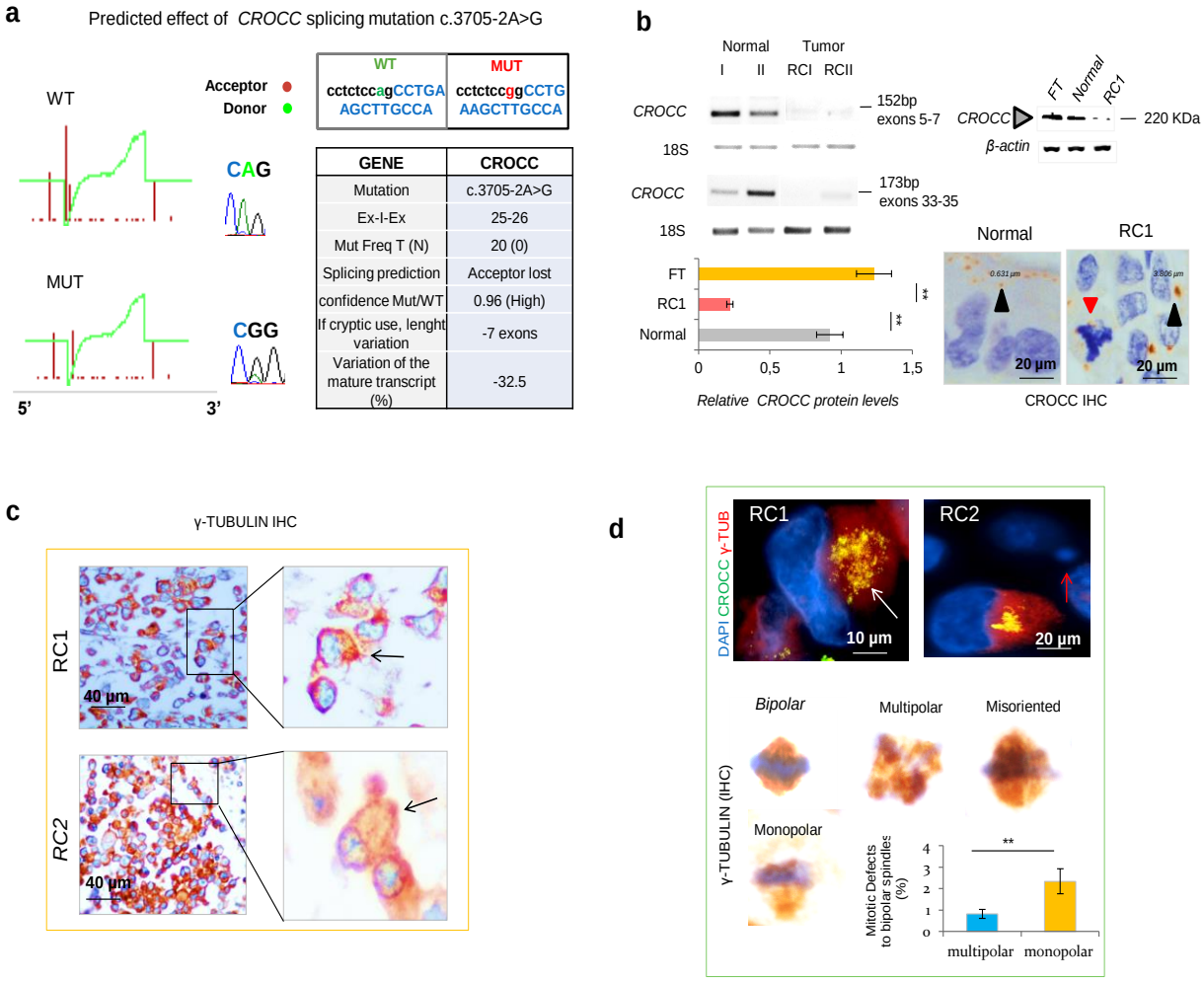

Extended data Fig 3. Effect of *CROCC* mutations on centrosome phenotype. **a** Bioinformatics prediction of *CROCC* mutation c.3705-2A>G at the 3' acceptor splice site in exon 25 using Splicefinder tool and Sanger sequencing validation. **b** The panel on the left shows *CROCC* RT–PCR-derived transcript products resolved on an agarose gel; the panel on the right shows CROCC protein expression by immunoblotting or immunohistochemistry from paraffin embedded rhabdoid colorectal cancer samples (RC), matched non neoplastic colonic mucosa (normal), and fallopian tube (FT) used as positive control. Centrosomes marked for CROCC are larger than normal (0.631 vs 3.806 µm, black arrowheads) or fragmented during mitosis (red arrow). Relative levels of CROCC expression to β-actin are shown. Data shown as mean ± standard error of the mean (s.e.m.) of 3 biological replicate, $^{**}P<0.01$, two-tailed Student's t-test. **c** Examples of abnormal mitotic spindles (black arrowheads) stained by immunohistochemistry (IHC) with anti-γ-tubulin antibody. **d** Upper panel, representative double immunofluorescence images from paraffin embedded sections reveal a marked loss of cell polarity and centrosome abnormalities (white arrow) or large micronuclei (red arrow). Lower panel, quantitative analysis of the number of abnormal spindles in both tumors, (>10 mitoses were included in the estimation in triplicate independent sections per tumor and related to the number of bipolar mitosis, error bars represent mean ± standard error of the mean (s.e.m) $^{**}P<0.01$, two-tailed Student

Extended data Fig. 4

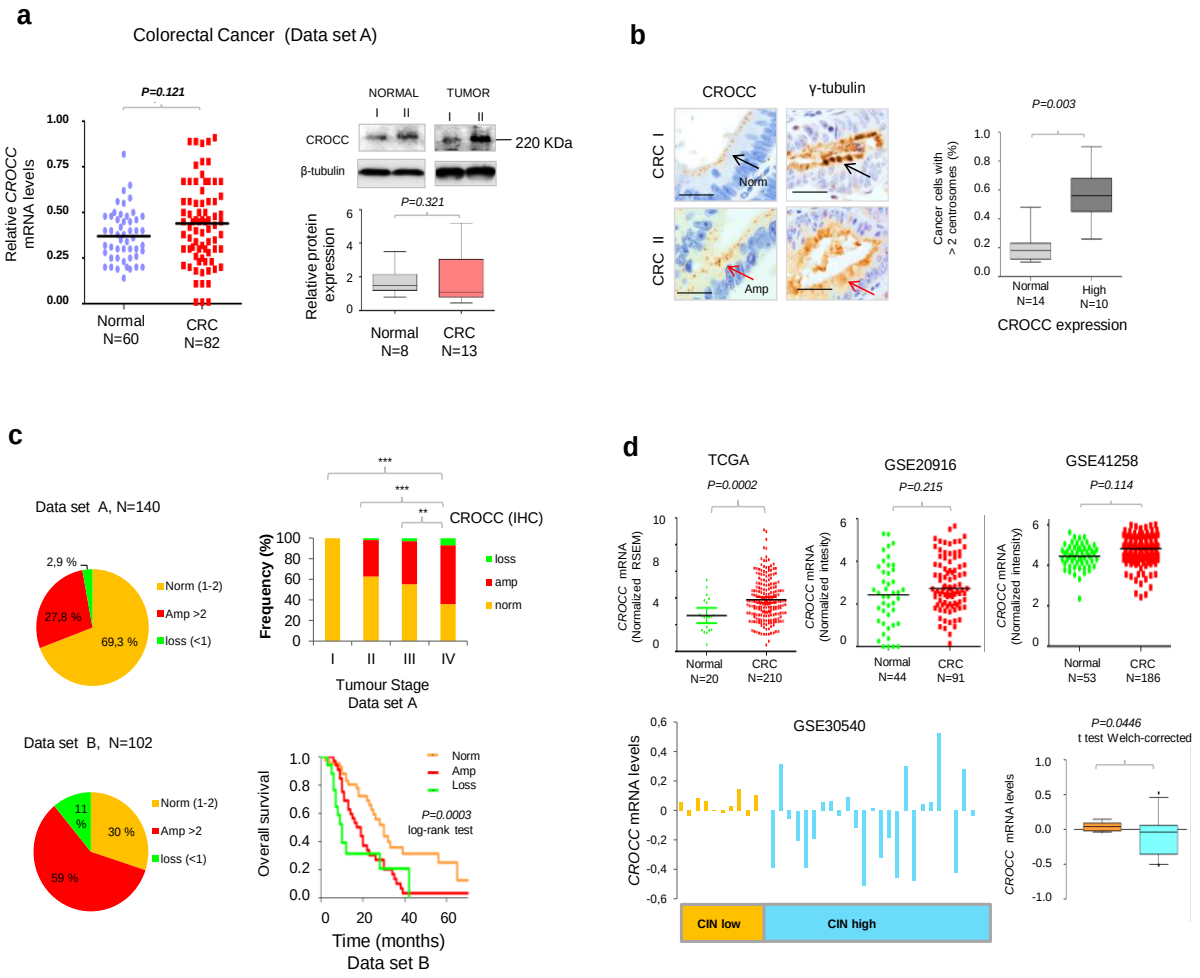

Extended data Fig 4. *CROCC* expression profiling in classical colorectal cancers (CRCs). a On the left, CROCC *mRNA* expression (qPCR) in CRCs and matched normal mucosa from a subgroup of 82 non-selected snap-frozen tumour and 60 normal tissues ("data set A" in the paper), *P value* from two-tailed Student's *t* test. On the right, representative immunoblot analysis from two CRCs and matched non neoplastic colonic mucosa (normal); the Box plot shows *CROCC* protein expression to β-actin from a subgroup of 13 unselected snap-frozen tumour and 8 normal tissues (data set A), of (*P value* from two-tailed Student's t-test). **b** Photomicrographs of CRCs immunostained for CROCC and γ-tubulin; lesions with a normal number (black arrow) or with supernumerary centrosomes (red arrow) are shown (Scale bars, 50 µm); the Box plot shows that samples with high CROCC expression display a higher percentage of cells with supernumerary centrosomes than those with normal CROCC expression (*P value* from two-tailed Student's t-test). **c** Centrosome numerical abnormalities including lack (<1 signal for cell) or supernumerary (>2 signals per cell) are related with tumour stage (Data set A) and overall patients' survival in (Data set B). *P values* determined by chi-square and log-rank test, respectively, ***P<0.01; ***P<0.001*. **d** Upper panels are Box plots of *CROCC* expression in colorectal cancer using patient-matched tumor-normal mucosa available from The Cancer Genome Atlas (TCGA) including n=210 patients and two Gene Expression Omnibus (GEO) data sets respectively including n=91 and n=186 patients. Low, on the right is shown the relationship between *CROCC* mRNA expression and cancers with high vs. those with low chromosome instability (CIN). Tumors were defined as CIN high or low based on a weighted genome integrity index (see Methods). *P value* determined by t test Welch-corrected.

Extended data Fig. 5

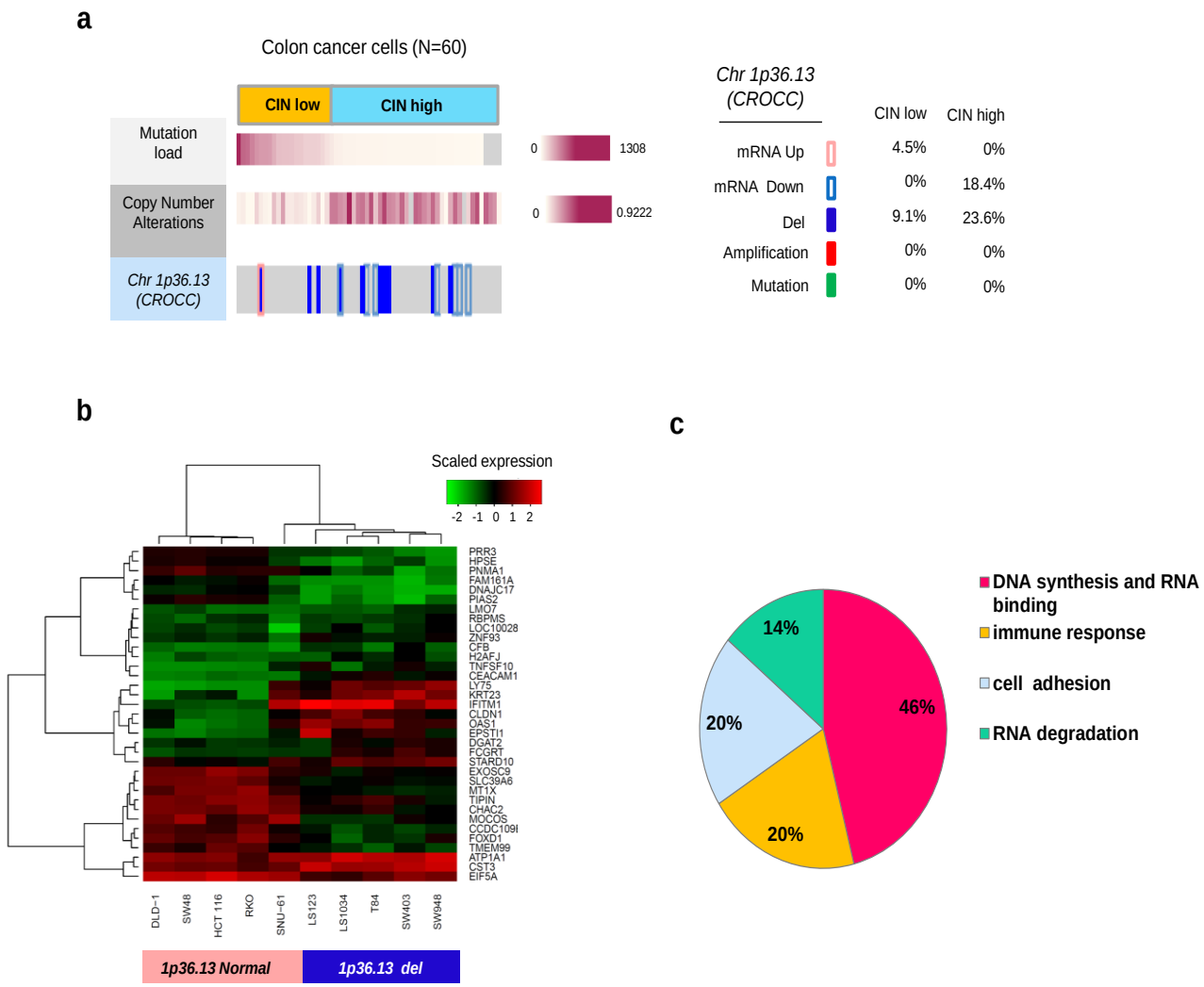

Extended data Fig 5. Allelic loss at the 1p36.13 locus correlates with chromosomal instability in colorectal cancer cells. a *In-silico* analysis identifies genetic deletion at the "1p36.13" locus where *CROCC* gene resides in CIN high versus CIN low colorectal cancer cells (Novartis/broad cancer cell lines encyclopedia); variation in the *CROCC* transcript are arbitrary fold change cut-offs of ≥2. **b** Heatmap of genes that are differentially expressed in colon cancer cells with or without 1p36.13 deletion. red, upregulation, green, downregulation. **c**, Gene ontology (GO) enrichment analysis for the differentially expressed genes.

Extended data Fig. 6

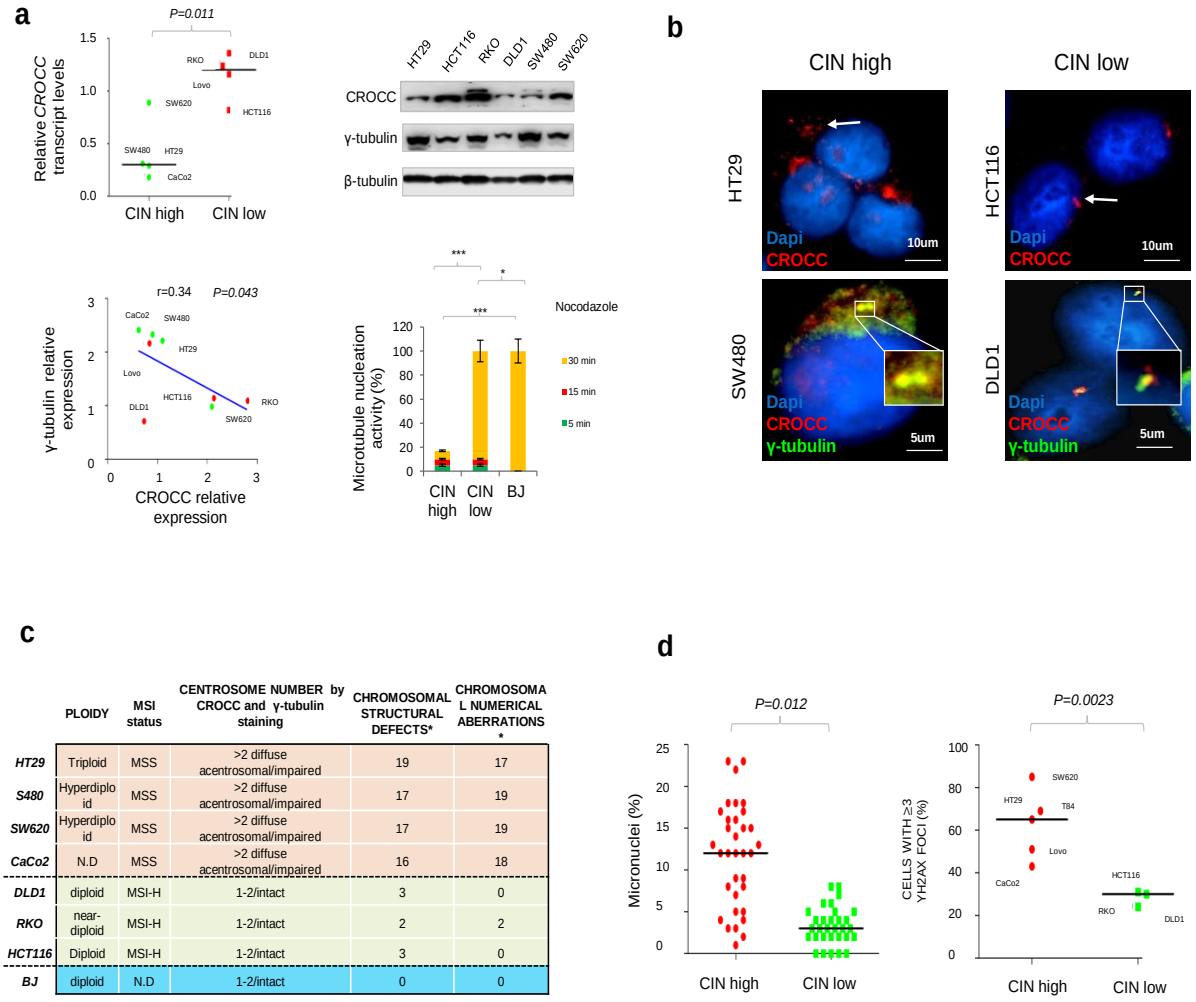

c

	PLOIDY	MSI status	CENTROSOME NUMBER by CROCC and γ-tubulin staining	CHROMOSOMAL STRUCTURAL DEFECTS*	CHROMOSOMAL NUMERICAL ABERRATIONS *
HT29	Triploid	MSS	>2 diffuse acentrosomal/impaired	19	17
S480	Hyperdiploid	MSS	>2 diffuse acentrosomal/impaired	17	19
SW620	Hyperdiploid	MSS	>2 diffuse acentrosomal/impaired	17	19
CaCo2	N.D	MSS	>2 diffuse acentrosomal/impaired	16	18
DLD1	diploid	MSI-H	1-2/intact	3	0
RKO	near-diploid	MSI-H	1-2/intact	2	2
HCT116	Diploid	MSI-H	1-2/intact	3	0
BJ	diploid	N.D	1-2/intact	0	0

Extended data Fig 6. Centrosome and chromosome instability in colorectal cancer cells. a On the upper left, quantification of *CROCC* mRNA (qPCR) expression levels in a panel of colorectal cancer cell lines classified as CIN high versus CIN low (see methods). Each *circle* represents the mean value of five biological replicates from each cell line, *p value* from two-tailed Student's t-test. On the upper right, the immunoblotting analysis of CROCC and γ-tubulin related to β-tubulin is shown. On the lower left, Spearman's rank correlation between CROCC and γ-tubulin protein expression; each *circle* represents the mean value of three biological replicates from each cell line. On the lower right, time-course analysis at 5, 15 and 30 minute (n>100 per cell line) after nocodazole removal of microtubule stained with anti γ-tubulin antibody in CIN high (HT29, S480, SW620, CaCo2), and CIN low (DLD1, RKO, HCT116) cancer cells; the graph shows that CIN high present a severe impairment of microtubule nucleation at 30 min as compared to CIN low cells, *P<0.001****, *P<0.05**, two-tailed t-test. **b** Immunofluorescence of CROCC (white arrows), is presented. DNA was stained with DAPI, the insets show enlargements of diffuse and delocalized staining or dot-like centrosomal structure in SW480 and DLD1 respectively, co-stained with CROCC (red) and γ-tubulin (green). **c** Summary of ploidy, centrosome abnormalities based and chromosomal aberrations in cancer cells. BJ are used as control. **d** Left, percentage of micronuclei in (HT29, S480, SW620) and (DLD1, RKO, HCT116) cancer cell lines. Percentage of γH2AX foci (right) in CIN high versus CIN low cells. Each circle represents the mean value of three biological replicate(n>100 per cell line). *P values* determined by two-tailed *t-test.*

Abbreviation: CIN, chromosomal instability; MSI, microsatellite instability; MSS, microsatellite stable; *Total number of chromosome abnormalities (structural and numerical changes) are included according to Barretina et al, ref 25.

Extended data Fig. 7

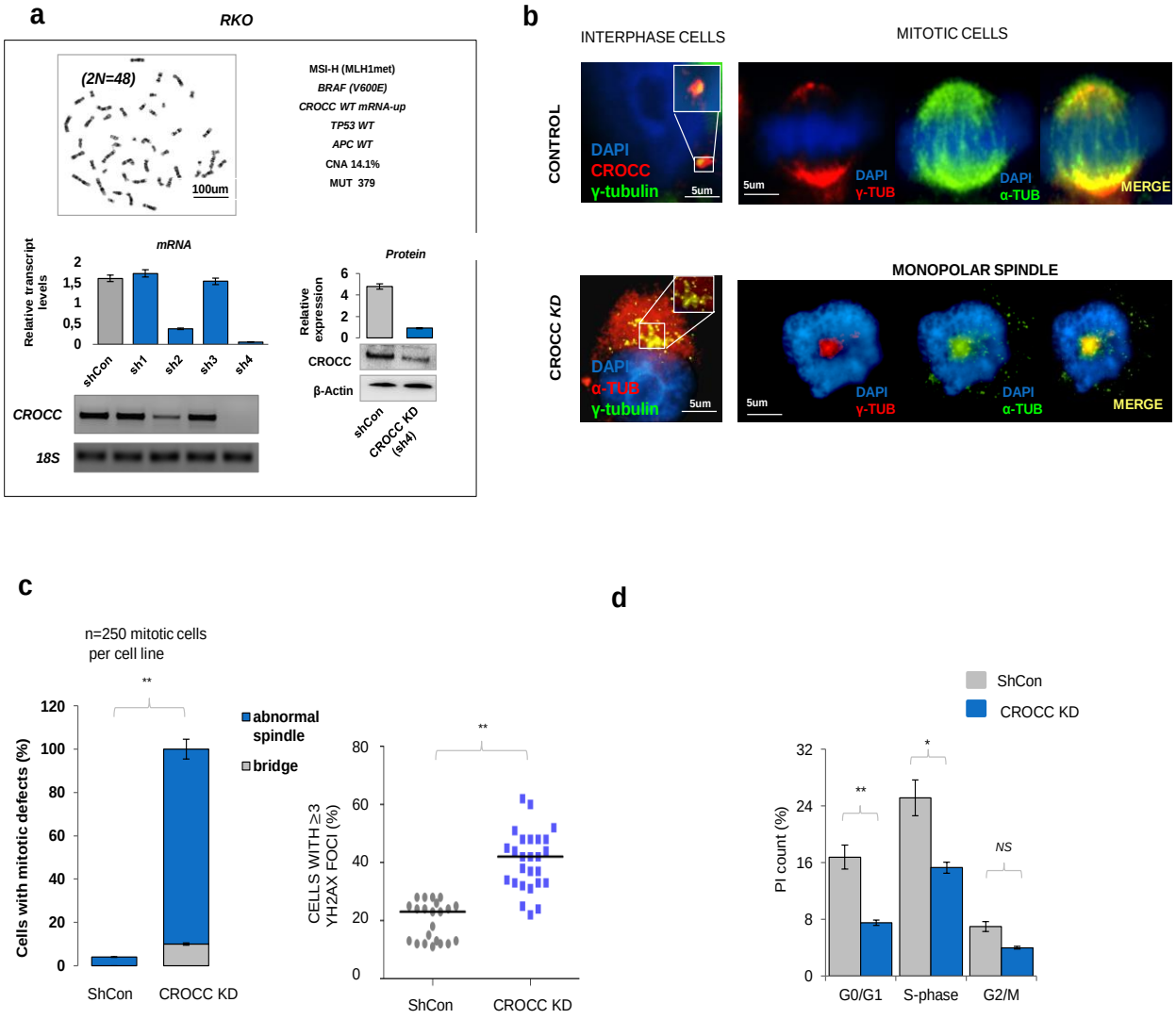

Extended data Fig 7. Mitotic errors and impaired cell cycle caused by stable *CROCC* depletion in RKO cells. a Upper left panel, karyotype of RKO cell line; upper right panel, genotypic characteristics of RKO cell line. Lower left panel, semi-quantitative CROCC mRNA RT-PCR and CROCC immunoblot after transfecting RKO with short-hairpin (shRNA) plasmids (sh1-4) targeting different regions of the *CROCC* mRNA; a control plasmid (shCon) demonstrates the absence of nonspecific off-target effect; the immune blot confirms that the most efficient inhibition is obtained with the sh4 clone. **b** Representative images of centrosomes for interphase or mitotic cells in RKO (shCon) and CROCC knock-down (KD or sh4) are shown. **c** quantification of mitotic defects (abnormal spindle including monopolar, multipolar spindle and polarity defects) and γH2AX foci in prometaphase in control and CROCC silenced cells are shown (Data are mean ± standard error of the mean (s.e.m) of biological replicates, *P<0.01***, two-tailed t-test relative to control). **d** cell cycle distribution analysis by propidium iodide (PI) and flow cytometry**.** Data are mean ± s.e.m of three biological replicates, *P<0.01***, P<0.05**, two-tailed t-test relative to control. NS, not significant.

Supplemental Fig. 8

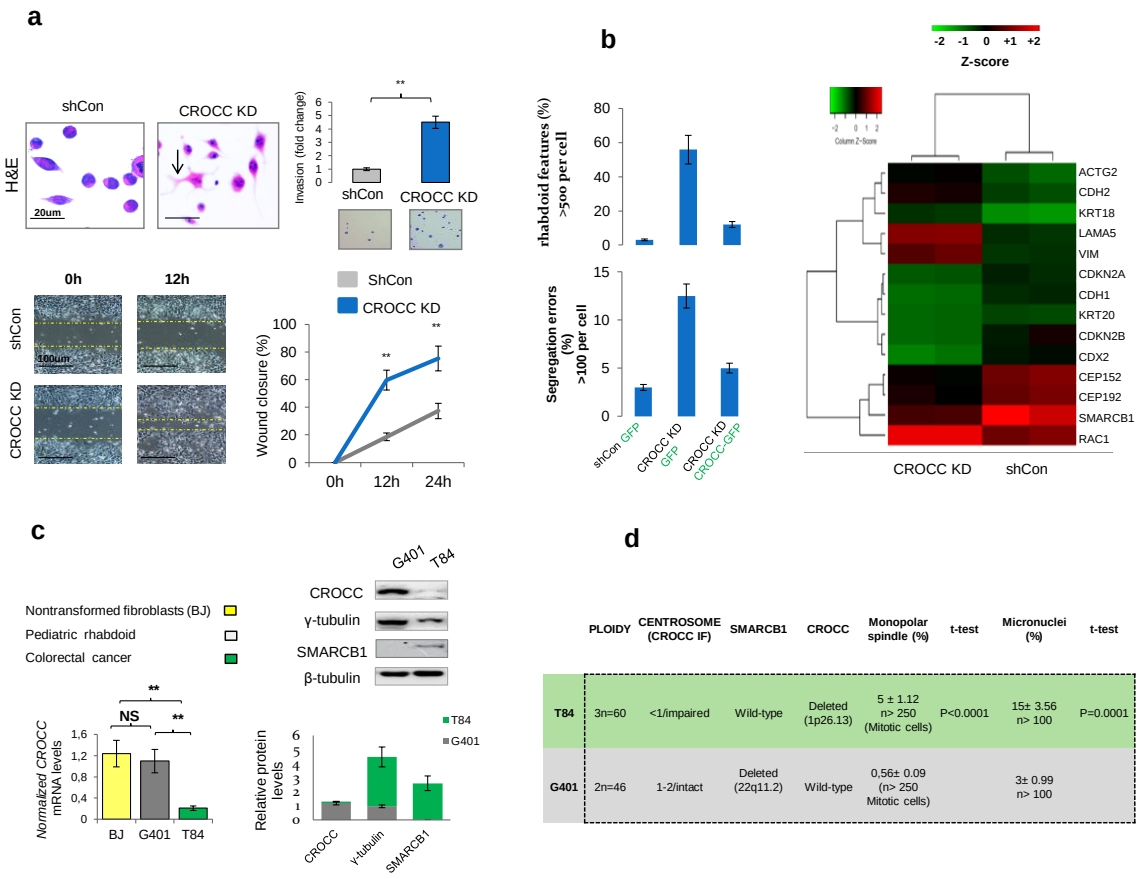

	PLOIDY	CENTROSOME (CROCC IF)	SMARCB1	CROCC	Monopolar spindle (%)	t-test	Micronuclei (%)	t-test
T84	3n=60	<1/impaired	Wild-type	Deleted (1p26.13)	5 ± 1.12 n> 250 (Mitotic cells)	P<0.0001	15± 3.56 n> 100	P=0.0001
G401	2n=46	1-2/intact	Deleted (22q11.2)	Wild-type	0,56± 0.09 (n> 250 Mitotic cells)		3± 0.99 n> 100	

Extended data Fig 8. Invasive behavior of colorectal cancer cells triggered by *CROCC* depletion. a Upper left, images show cells transfected with control plasmid (ShCon) or CROCC knock down (KD) plasmids stained with Hematoxylin&Eosin (H&E) (scale bar: 20 µm); the black arrow points to invasive protrusions in cells silenced for *CROCC*. Upper right, quantification of invading cells by matrigel invasion assay in serum-free DMEM. Lower panel, microphotographs of wound healing assay (scale bar: 100 µm) and graph of wound closure timing (mean values ± standard error of the mean (s.e.m) of three biological replicates. *P<0.01***, *P<0.05**, two-tailed t-test relative to control). **b** left, shCon and *CROCC*-KD cells were transfected with GFP or CROCC-GFP and analyzed for the number of rhabdoid cells and percentage of segregation errors (n≥25 anaphases per experiment). Data are mean+s.e.m of three independent experiments. Right, heatmap of differentially expressed genes involved in epithelial mesenchymal transition and centrosome/cytoskeleton mediators (mean values of three biological replicates are shown for each condition. Red, upregulation; Green; downregulation). **c** quantitative RT-PCR of the relative *CROCC* transcript in the indicated cell lines, and immunoblot analysis of CROCC, γ-tubulin and SMARCB1 related to β-tubulin. The histogram on the lower right shows the relative abundance of each protein by immunoblot analysis in the indicated cancer cell lines (Data are mean ± s.e.m. of three biological replicates, *P<0.01***, two-tailed t-test). **d** Distribution of centrosome defects as detected by CROCC immunofluorescence (IF), genetic defects (*SMARCB1 and CROCC* allelic losses), replication errors accounted for monopolar spindle errors (MSP) or micronuclei (Mn) (mean ±s.e.m., n=3 experiments)

Supplemental Fig. 9

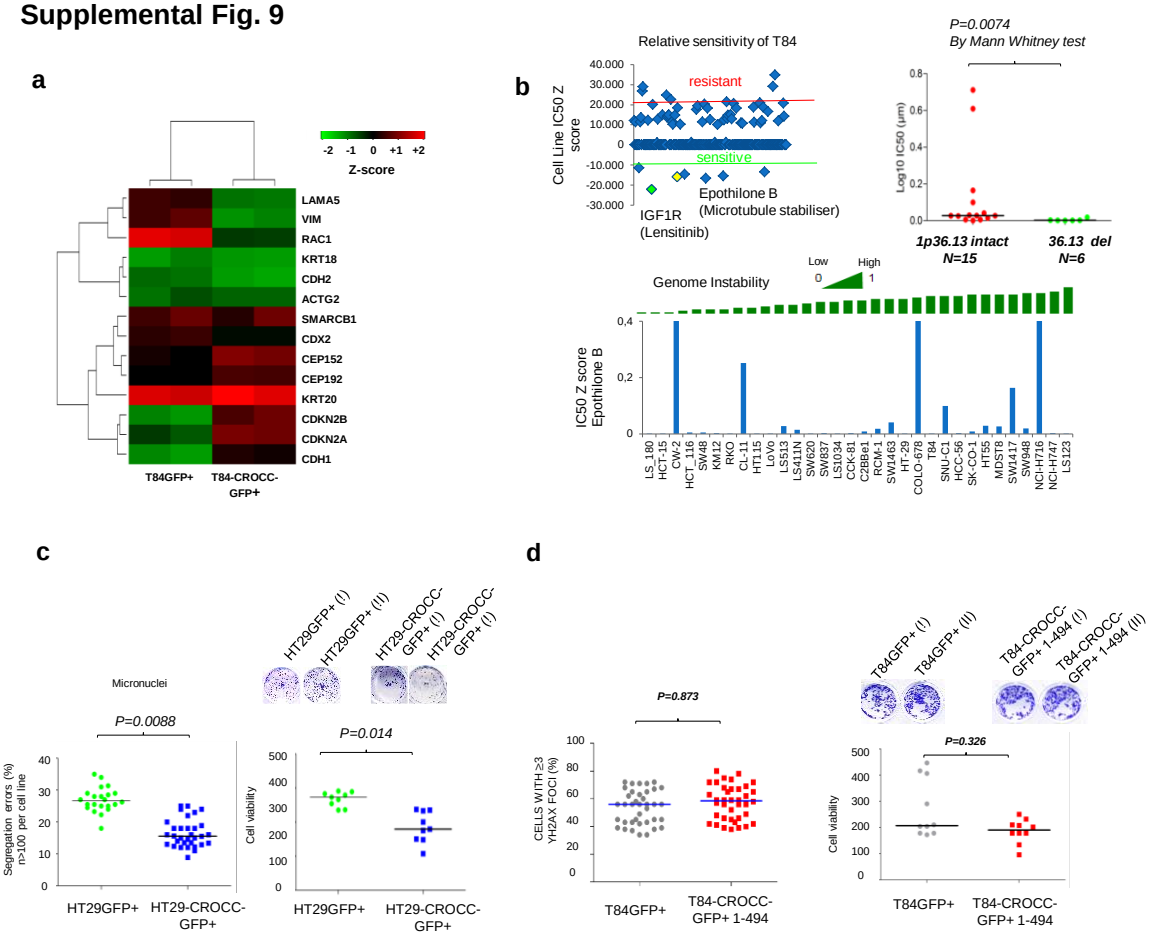

Extended data Fig 9. a Mitotic aberrations suppressed by *CROCC* or microtubule stabilizing agents in metastatic T84 and HT29 colorectal cancer cells. **a** Heatmap of differentially expressed genes following *CROCC* rescue in T84 cells (mean values of three biological replicates are shown for each condition. Red, upregulation; Green; downregulation). **b** Dispersion plot of IC50 values for treatment of T84 cell lines with 222 different molecules extracted from the Genomics of Drug Sensitivity in Cancer project. In green and yellow are indicated the top 2 most effective drugs. Log_{10} IC50 values for treatment of 1p36.13 intact and 1p36.13 deleted cell lines with Epothilone B. Below, Epothilone B "a microtubule stabilizing agent" IC50 results comparing CIN-low vs. CIN-high CRC cells. **c** On the left, the percentage of micronuclei in HT29 cells transfected with full-length human CROCC-GFP or GFP alone used as control (*P value* by Mann–Whitney U test). Right, viability was assessed by a colony formation assay. The cells were fixed, stained, and photographed after 12 days of culture. **c** The left graph reports flow cytometry analysis after 6 days, (*P* value by two-tailed Student's t-test). **d** Left, effect of a *CROCC* mutant form (1-494) on the formation of γH2AX foci, (n>100 per cell line; *P value* determined by two-tailed t-test relative to control). Right, representative images (top) of cells assessed by a colony formation assay, fixed, stained, and photographed after 10 days of culture; the graph below shows the distribution of cell viability by colony formation assay obtained by five biological replicates per cell line (*P value* determined by two-tailed t-test relative to control).